Two-dimensional Shock Sensitivity Analysis for Transonic Airfoils with Leading-Edge and Trailing-Edge Device Deflections

Michael M. Henry

Thesis Submitted to the Faculty of
the Virginia Polytechnic Institute and State University
In partial fulfillment of the requirements for the degree of

Master of Science
In
Aerospace Engineering

W.H. Mason, Chair
J.A. Schetz
B. Grossman

20 August 2001
Blacksburg, Virginia

Keywords: transonic airfoil, device deflection, shock movement, 2-D flow separation

Table of Contents

List of Figures

Acknowledgements

This research was supported by the Office of Naval Research (grant# N0014-99-1-0846) through Dr. W. H. Mason and the Department of Aerospace and Ocean Engineering at Virginia Polytechnic Institute and State University. The support is gratefully acknowledged. I would also like to thank Darren Grove of the Navy for personally providing the three-dimensional CFD grid and solution files, as well as Charlie Swanson from LaRC for providing the grid generating and flow analysis codes. There are two groups that I would like to thank for their support through the past six years. Those who have supported me without understanding exactly what I've been doing, and those who have supported me by helping me understand what it is I'm doing.

Chapter 1: Introduction

The phenomenon known as “wing drop” was identified several years ago and still remains the source of much curiosity, as well as the motivation for this investigation. Wing drop tendencies have been noted on several existing aircraft with a variety of configurations, from the F/A-18E/F to the NASA F-111 TACT.[1] Many aircraft encounter a form of wing drop at high angles of attack, which is not the focus of this investigation. The aircraft mentioned above, in early development stages, have encountered wing drop at relatively low angles of attack. This results in unexpected forces in the middle of the operational envelope. Ultimately, the cause of this phenomenon is asymmetric separation on the wings of the aircraft. The result is an asymmetric lift producing a sudden and uncommanded rolling moment.[2] Considering the fact that each wing is exposed to relatively similar airflow conditions, it can be assumed that only a slight variation in flow is causing the sudden increase in the separation region on one wing.

Investigation of this phenomenon requires a breakdown of the three dimensional components of the complicated wing. This particular study is focused on the two dimensional airfoil incorporated in the wing of an aircraft that frequently encountered wing drop in its development phases. An investigation of the flow characteristics is aimed at the sensitivity of the airfoil to changes in the encountered flow (i.e. Mach number and angle of attack).

In particular, the movement of the shock wave is of special interest. The recompression that occurs across the shock wave is a major contributor to flow separation. A similar airfoil, one from an aircraft wing that does not exhibit strong wing drop tendencies, was used for comparison purposes.

In addition to the comparative study for these two airfoils, it was desired to investigate the role of the leading edge and trailing edge devices on the airfoil. Control surfaces give a symmetric airfoil variable camber and increase its performance over a range of design conditions. However, altering the shape of the airfoil alters the behavior of the shock movement and separation region.

Of particular interest is the interference of the flow pattern caused by the hinge-lines.[3] A combination of the shock wave and the trailing edge pressure gradient have a tendency to thicken the boundary layer so that small flap deflections can lead to separation.[4] The details of this type of *corner flow analysis* can be found in the papers of Mason[3] or Chung[5]. It is the overall behavior of this separation region that is of interest for this particular study.

Chapter 2: Airfoil Geometry

Selection from 3D Wing

To do a two dimensional analysis that would be relevant, it was critical to select an airfoil directly related to wing drop problems. Three dimensional CFD data provided by the Navy made it possible to match the geometry of a generic airfoil with one used in an existing, moderately swept, wing that had exhibited wing drop during early development testing. Figure 1 shows the separation progression on the upper surface of this wing. The red areas correspond to reversed axial flow and the blue regions indicate positive axial flow. Note the large increase in separation between 6^o and 8^o, indicating a rapid forward movement of the shock together with separation. There is no guarantee that the blue regions are entirely attached flow, but the assumption is sufficient for selecting the spanwise position of interest for the two-dimensional investigation. It is important to note the expansion in the region of separation near the midspan of the wing. An investigation of the isobars in this region shows that the flow here is essentially unswept. It is the combination of airfoils that make up this section of the wing that are of interest for this analysis. A cross section of the spanwise location indicated by the black line in Figure 1 was used to select the airfoil used for the two dimensional analysis, presented here.

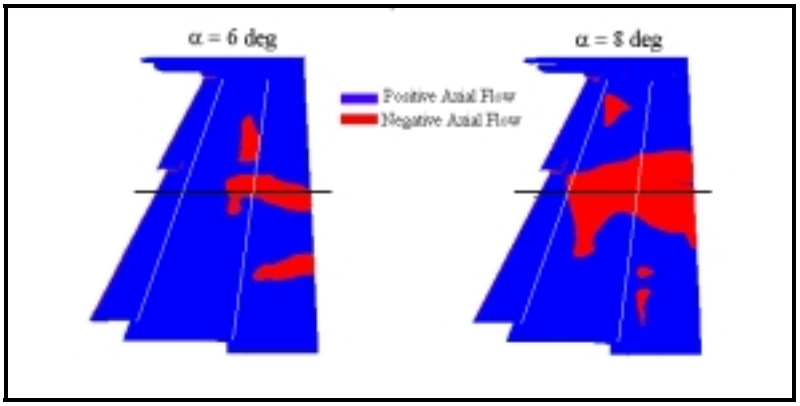

Figure 1: Directional flow patterns (M = 0.8)

Description of Airfoil

The airfoil used in this particular section of the wing closely resembles a NACA 65A series airfoils with a thickness to chord ratio of 5.7% (NACA 65A005.7). The flap schedule used in this CFD code was matched with that for a wind-up-turn maneuver. It is under these conditions that wing drop was found for early configurations of this particular aircraft. For this spanwise position the leading edge is deflected down approximately 10^o and the trailing edge is deflected down 9^o. The original, uncambered airfoil was obtained by means of the airfoil generating code known as **LADSON**[6].

The output from this code includes a list of the two-dimensional airfoil coordinates. These coordinates were then altered near the leading and trailing edge to match the shape of the original three-dimensional cross section with device deflections. With the aid of a spreadsheet, the coordinates for the leading 15% of the airfoil were rotated 9^o down. Similarly the coordinates for the trailing 30% of the airfoil were rotated down 10^o. With these deflections, as seeen in Figure 2, the NACA 65A airfoil more closely matched the airfoil extracted from the three-dimensional wing.

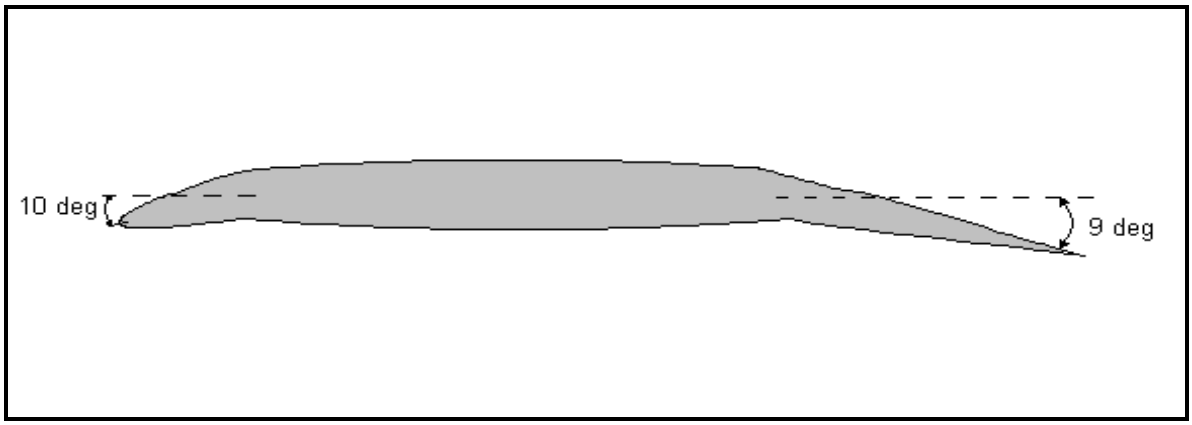

Figure 2. NACA 65A005.7 with deflected surfaces

Chapter 3: Airfoil Analysis Methodology

Here we describe the methodology used in the two dimensional analysis. The size and coarseness of the grid, the turbulence model, and the convergence sequence are all variables that must be considered in the validity of any two-dimensional results.

Generating the Grid

The process of analyzing the two dimensional airfoil began with generating a grid that encompasses the airfoil. The grid generating package consists of three programs that construct a C-mesh around the input airfoil coordinates. **Gair2** is the first of the codes, which defines the surface points for the c-mesh. **Hyperg2** is then used to solve two equations, one enforcing orthogonality and the other maintaining constant cell area for a line of cells around the airfoil. This is the actual grid generating process. The final code, **printn**, is used to organize the grid points in a file for visualization.[7]

This grid generating code is capable of producing a mesh of any size prescribed by the user. For the NACA 65A series airfoils, a 480 x 64 cell grid was constructed. This means that the grid is assigned to 480 cells on the surface of the airfoil, and 64 cells perpendicular to the surface. In addition to the cells surrounding the airfoil there are also 64x64 cells that make up the wake region behind the airfoil. A critical option in the input file for the grid generating code deals with the assignment of the distribution of surface cells. Proper manipulation allows the user to concentrate the cells in regions of interest. For regions of changing geometry, such as around the nose, this produces a more accurate analysis. Notice in Figure 3, the concentration of cells around the nose in comparison to the larger less abundant cells at the mid-chord region, where the geometry varies in a less abrupt manner.

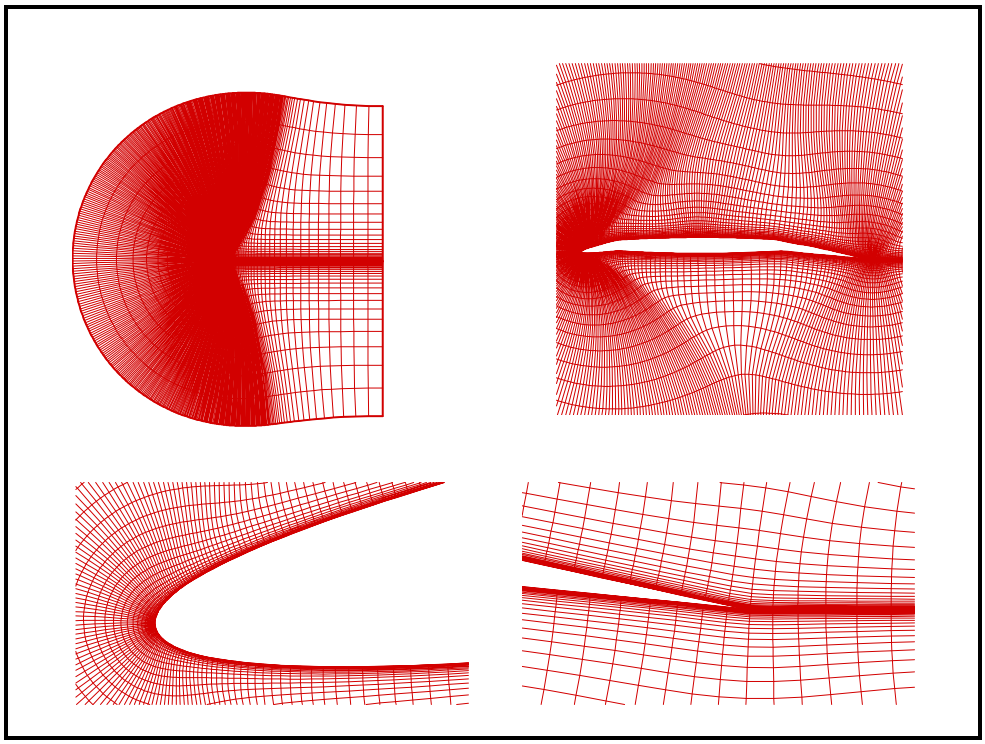

Figure 3. Grid for NACA 65A005.7

Generally, for a turbulent analysis it is desired to have a grid with normal grid points starting inside the laminar sublayer ($y^+ < 10$, where $y^+ = yu^*/\nu$). The grid used in this study had relatively large y^+ values for the first gridpoints off the surface, extending up to $y^+ \approx 30$. When this was discovered another grid was generated with grid points much closer to the surface of the airfoil. The new grid had gridpoints ¼ of the distance off the airfoil compared to the original grid. This produced y^+ values within the laminar sublayer, but the results of the calculated pressure distributions were very similar as seen in Figure 4. There was a slight variation in the quantitative results, but the behavior of the changing pressure distribution was similar. Since the focus of this study is on the shock behavior, the original grid is sufficient for the investigation.

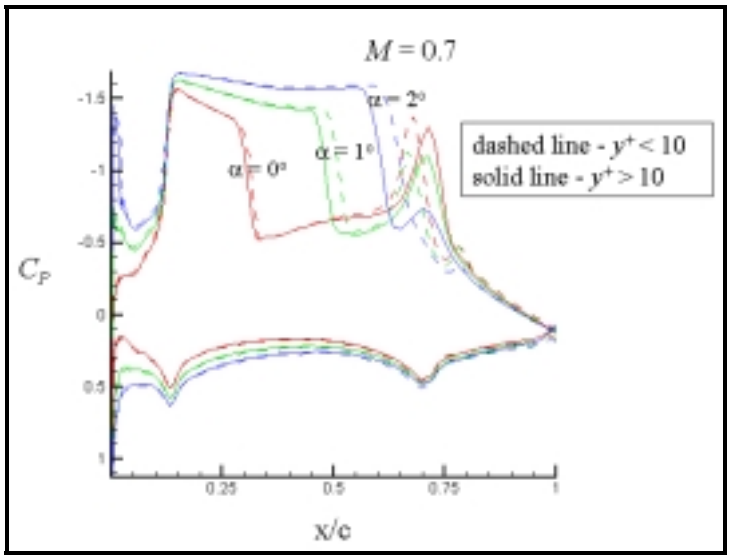

Figure 4. Grid comparison through C_P distributions, showing the effect of assigning grid points within the laminar sublayer

Flow Analysis

FLOMG[8], a two dimensional analysis code provided by NASA Langley, was used to produce the aerodynamic data for all airfoils. This code is "based on central differencing and Runge-Kutta time stepping. It uses a multigrid method and variable coefficient implicit residual smoothing for convergence acceleration."[8] **FLOMG** approximates the flow based on the solutions of unsteady Euler or Navier-Stokes equations. There are several options for running the **FLOMG** code. It can be run using a thin layer Navier-Stokes solution, or turbulence models can be incorporated. The program can use either the Baldwin-Lomax[9] or Johnson-King[10,11] turbulence model. The results in this report were obtained by using the former of these two models.

As mentioned above, **FLOMG** uses a multigrid method to accelerate convergence. There were three multigrid levels used for this particular analysis. Limitations of this program in converging for relatively high Mach numbers and angles of attack prevented us from obtaining solutions for some conditions. Convergence can be interpreted through several variables in the output files. The easiest variable to follow in convergence is the residual itself, which should be decreasing to zero assuming the approximation is converging on a solution. Convergence of the residual should be accompanied by other variables, such as the lift coefficient. If the lift coefficient is not converging to a constant value, then a converged solution has not been found. Figure 5 shows the difference between a converging and non-converging case. Convergence time varied with each case, and depending on the complexity of the flow, would take anywhere from twenty minutes to just over an hour to produce results. These times estimates are based on the performance of an

Origin 2000 with 16 195mHz MIPs R10000 CPUs, and 16 250mHz CPUs. This is a computer of the Virginia Tech ICAM (Interdisciplinary Center for Applied Mathematics) computer system, which was used to process the **FLOMG** code. With the output from **FLOMG** and the post processing code, **pltcon**, it is possible, using Tecplot®, to produce velocity profiles, streamtraces, Mach number variation, pressure profiles, and density contours for any given airfoil.

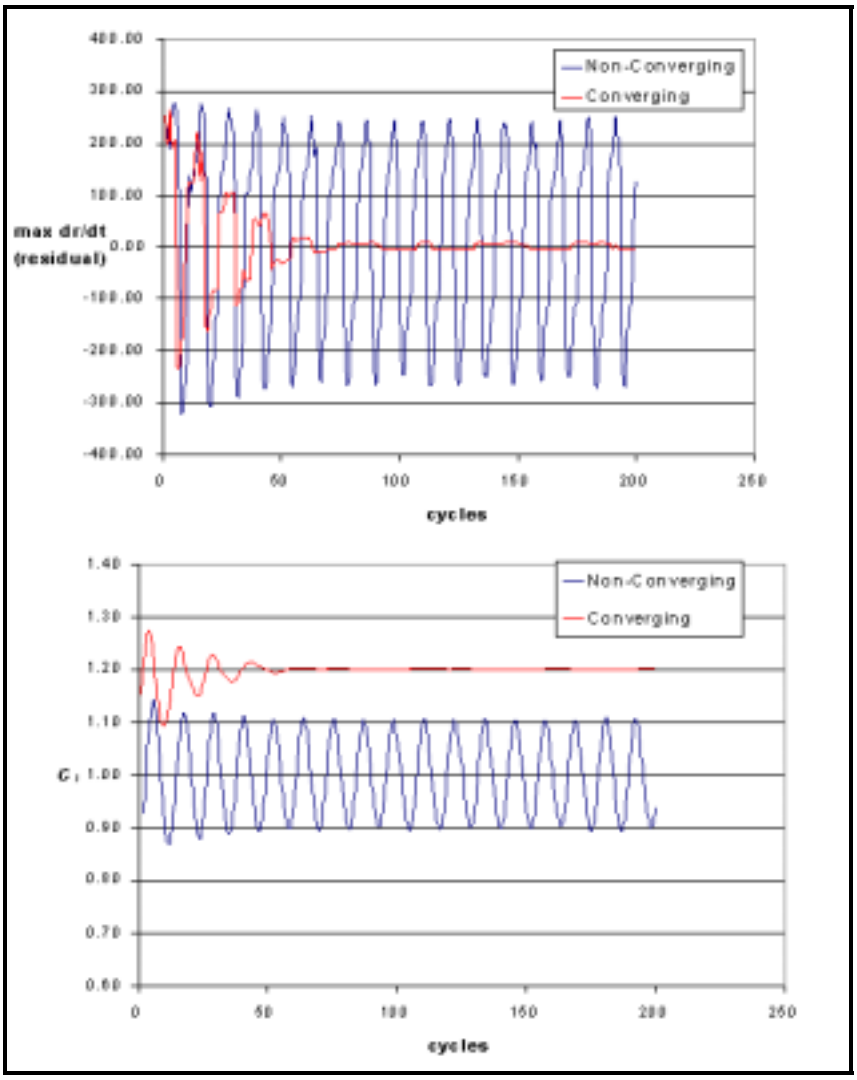

Figure 5. FLOMG Output: convergence vs. non-convergence

Turbulence Models

It was stated in the previous section that the **FLOMG** code contains the option of using a Baldwin-Lomax or Johnson-King turbulence model. The significance of which turbulence model is used can not be determined without data from each case to compare. W.K. Londenberg[12,13]

published the results of an evaluative study on turbulence models in 1993. Included in Londenberg's study were the Baldwin-Lomax and Johnson-King turbulence models. Based on pressure distributions, both turbulence models produced results that "compared well" with the experimental data of an undeflected airfoil. However, once the control surfaces were deflected, the Baldwin-Lomax model produced less favorable results.

Terry L. Holst[14] showed in a transonic airfoil study that the Johnson-King turbulence model is capable of producing an upper surface pressure distribution very similar to that of experimental data for the NACA 0012 airfoil. Holst shows that the Baldwin-Lomax model fails to accurately predict the shock location on transonic airfoils, placing it consistently further aft than the data for the NACA 0012 airfoil. Holst notes in his study that one drawback of the Johnson-King model is an underprediction in the lower surface pressure distribution. As a result, the lift coefficient is low and drag polar results are actually less favorable then those predicted by the Baldwin-Lomax model. The lower surface pressure distribution and the drag polar plots are less significant than the accuracy in predicting the upper surface pressure distribution, at least in this particular investigation. It is the movement of the shock on the upper surface that is of primary concern. Therefore, the Johnson-King model, based on the studies of Londenberg, Holst, Johnson and Coakley[11], appears the be the better choice of these two turbulence models for a two dimensional analysis focused on the shock behavior.

Using **FLOMG**, two-dimensional data was collected for several cases of the 65A series airfoil using both the Baldwin-Lomax and the Johnson-King turbulence model. Overall, the results provided by the two turbulence models are comparable. There is a slight variation in the shock location, seen in Figure 6, as can be expected based on the studies of Holst, and Londenberg.

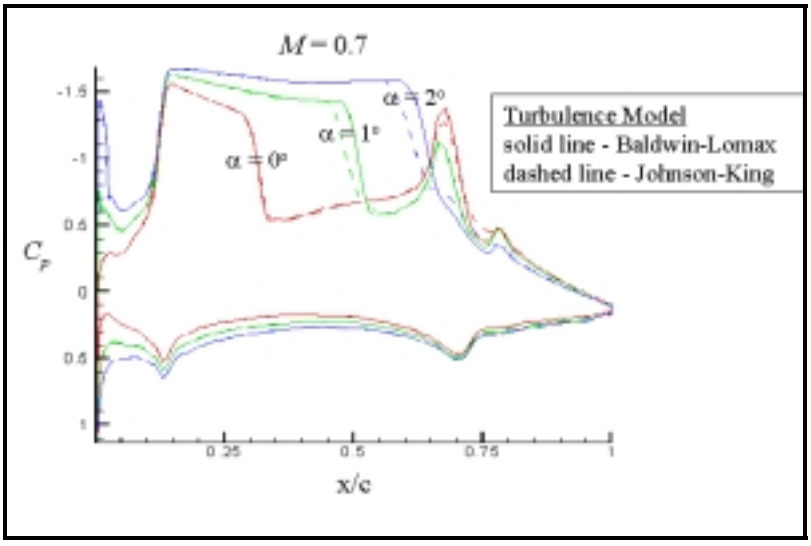

Figure 6. Turbulence model comparison

Without experimental data to compare, it is impossible to draw any conclusion as to which turbulence model is producing the most accurate results. Based on the comparison shown in Figure 6, it is safe to assume that for this airfoil both models produce qualitatively similar results. The variation, as mentioned above, is minimal and does not effect the pattern of the shock movement. If both turbulence models display a similar shock behavior, it is irrelevant which model is used for this investigation. However, for our study we could not get FLOMG to converge using the Johnson-King model at the higher Mach numbers. Thus, in this study we used the Baldwin-Lomax turbulence model.

Chapter 4: Investigation of Flow Characteristics for NACA 65A005.7 Airfoil

To compare a two-dimensional analysis with the three-dimensional case, it is necessary to match certain characteristics, preferably the lift coefficient. Analyzing the two-dimensional airfoil at the same Mach number and angle of attack as those of the three-dimensional case would not produce similar results. The lack of 3D effects requires that the Mach number and angle of attack be adjusted to produce flow characteristics (i.e. C_P and C_l) similar to the three-dimensional values. Figure 7 shows the three-dimensional pressure distribution in comparison with the two dimensional C_P distributions at select Mach numbers and angles of attack. Notice the difference between the three-dimensional C_P profile and the two-dimensional results for M=0.8 and $\alpha=6^o$. Clearly it is not acceptable to simply expose the two-dimensional airfoil to the same conditions as the three-dimensional wing. Through comparison, it was found that the two-dimensional airfoil exposed to Mach numbers from 0.7 to 0.8 and α's varying from 0^o to 2^o produced C_l values similar to the section lift coefficient extracted from the three-dimensional wing. Obviously we could pick a constant angle of attack and find the corresponding Mach number that produces a matching C_l value, but as seen in Figure 1 of Chapter 2 the separation increase on the wing occurs as a result of increasing angle of attack. Therefore, it was desired to focus primarily on a Mach number or range of Mach numbers that produce a lift coefficient similar to the three dimensional case at varied angles of attack.

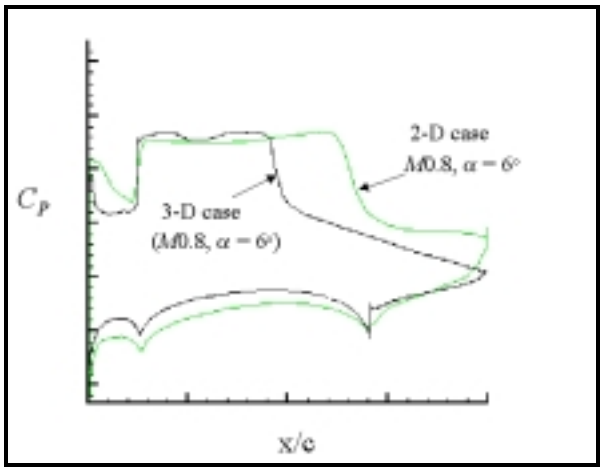

Figure 7: 2D and 3D C_P's for the same conditions, illustrating the need to use "equivalent" 2D M and α

It is clear from Figure 7 that the two-dimensional airfoil is producing a C_l higher than the corresponding three-dimensional case. This variation is interesting because it is due to the chord-wise location of the shock. It is the position of the shock and its migration that are of particular interest in this investigation.

The most important characteristic of the airfoil for this study was the movement of the shock wave as Mach number and angle of attack varied. The significance here is due to the fact that the sudden pressure recovery across a shock wave often results in separated flow. Therefore it is fairly easy to follow the separation on an airfoil surface by studying the migration of the shock wave. In this case, interest is focused on the possibility of a sudden shock shift forward or in essence an airfoil that is unusually sensitive to minor flow changes in a specific regime. For instance, does the 5.7% thick 65A series airfoil tend to display unconventional characteristics for conditions between M=0.7 and M=0.8. With this in mind, it seems most reasonable to examine the changing pressure distributions for the 5.7% airfoil.

Figure 8 shows the behavior of C_P and C_f with respect to increasing angle of attack (α) for M=0.7. For each α the initial expansion occurs at the same chordwise position, this is the location of the hinge-line for the leading edge control surface. This is the beginning of the supersonic flow region on the upper surface of the airfoil. The flow, in each case, remains supersonic for some stretch across the upper surface, until it encounters the shock wave where it returns to subsonic speeds. This shock location is clearly indicated in the C_P plots by the sharp recompression at the back side of the pressure "plateau".

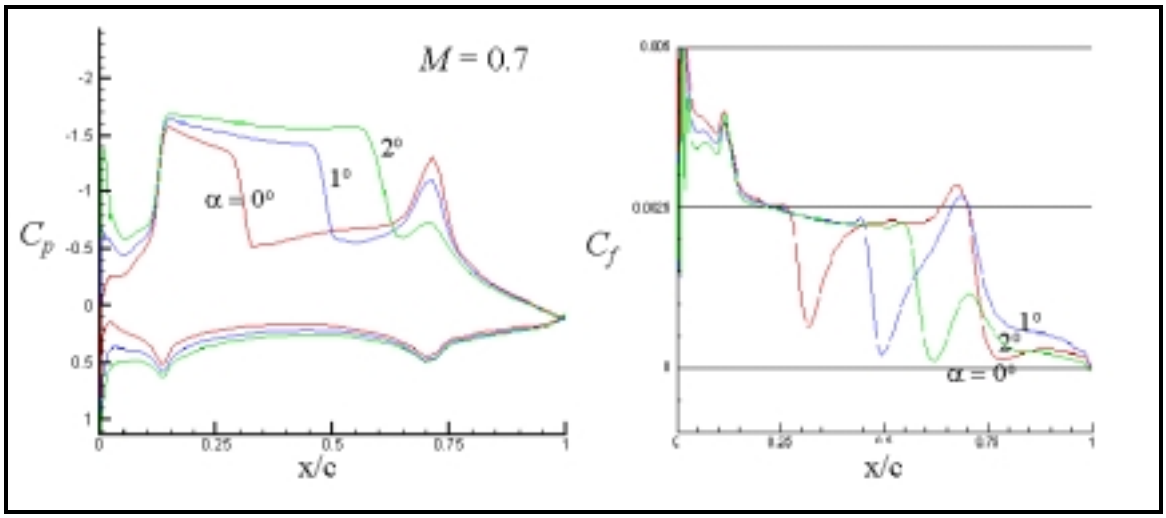

Figure 8. *Cp* and *Cf* vs α (*M*0.7)

For the $\alpha=0^o$ case the shock is just aft of the leading edge hinge-line containing the supersonic flow to a fairly small region. As α increases the shock moves aft fairly 'quickly'. At $\alpha=2^o$ the shock is almost as far back as the trailing edge hinge-line. One thing to notice is the expansion and recompression that occurs at the hinge-line for the trailing edge flaps. This is important for two reasons. It demonstrates the effect that the hinge-line has on the flow over the airfoil surface. Non-separated flow will not pass over the discontinuity formed at the joint without being affected. Another reason that this characteristic is significant is the fact that it is a clear indication that the flow is not separated at this point. If the flow were separated by the shock in any of these cases it would pass over this hinge-line without the expansion and recompression that is prevalent here, in other words, if a large region of separated flow occurs, it will not "see" the hinge-line.

As mentioned above, the flow remains attached in each case of Figure 8. This is verified by the skin friction plot on the right hand side. Sharp drops in the skin friction value correspond to the flow passing across the shock wave. The fact that C_f remains positive for all three cases verifies that the flow does not separate under these conditions.

Slightly increasing the Mach number(M = 0.725) for these angles of attack results in the pressure distribution seen in Figure 9. The shock has continued to shift towards the aft of the airfoil. For $\alpha = 0^o$ the shock is still only as far back as mid chord, and the flow remains attached as it passes through this shock. What is starting to become prevalent here can be seen in the location of the shock for the 1^o and 2^o cases. For these angles of attack, at M = 0.725, the shock has migrated all the way to the trailing edge hinge-line. Here it remains fixed for both cases.

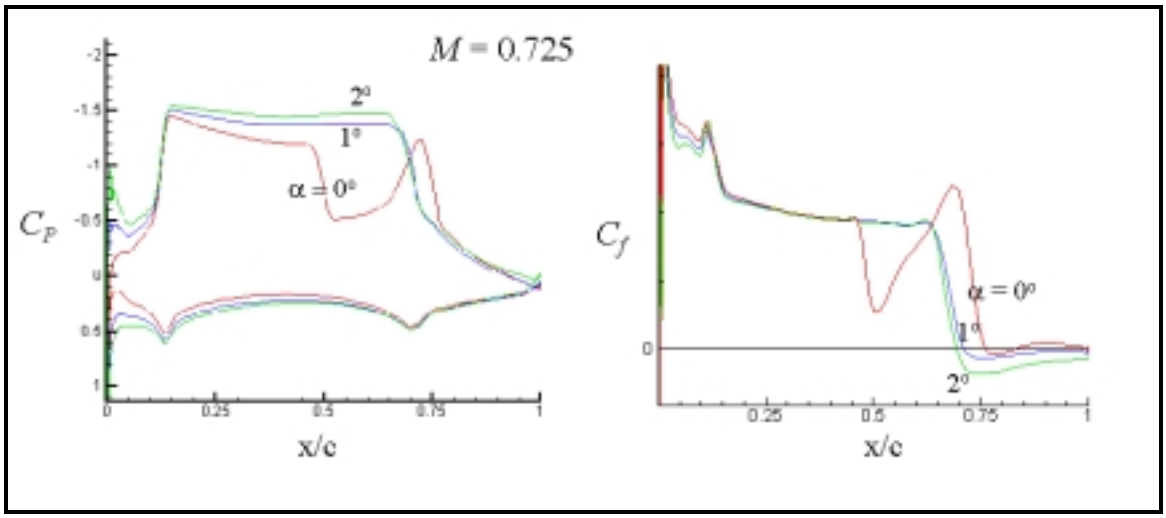

Figure 9. C_P and C_f vs α (M0.725)

The skin friction plot is beginning to show regions of separated flow at this Mach number. For all three cases there is some sign of separation, and in each case it occurs immediately following the pressure recovery at the trailing edge hinge-line. For the $\alpha = 0^o$ case the flow is able to reattach on the flap, but for the higher angles of attack, the flap is submerged in separated flow.

When the Mach number is to increased to 0.75, the shock for the $\alpha = 0^o$ case moves all the way to the hinge-line of the trailing edge, as can be seen in Figure 10. Here it becomes fixed and the pressure distributions for all three angles of attack begin to look very much the same. The shock has not moved for the 1^o and 2^o cases with respect to the previous Mach number. The flow at this Mach number is entirely separated on the upper surface of the flap for all three angles of attack.

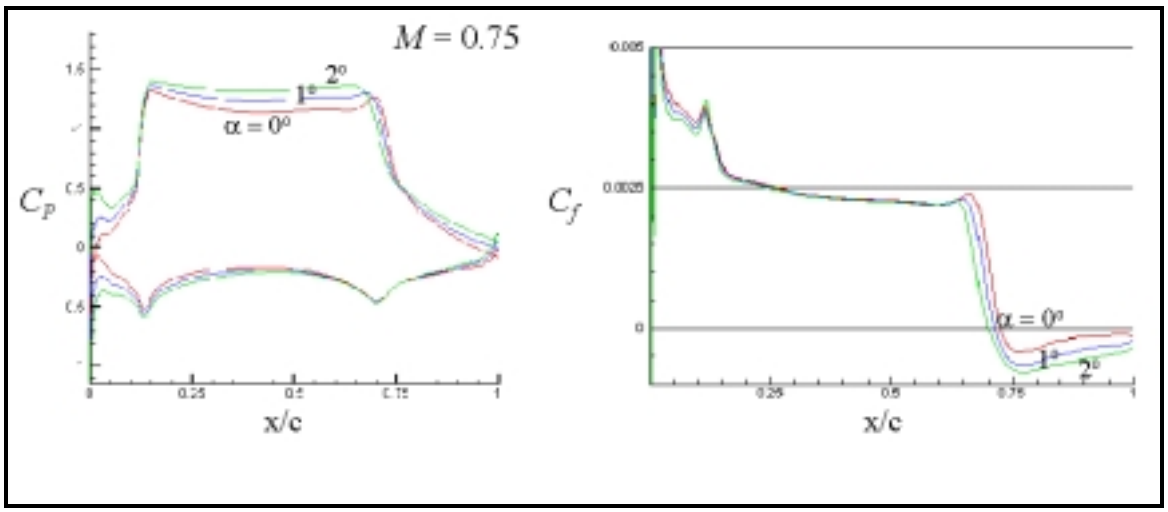

Figure 10. C_P and C_f vs α (M0.75)

Figure 11 and Figure 12 verify that the pattern seen in the previous plots continues for even higher Mach numbers. The most significant characteristic to notice in these plots is the fact that the shock has become stationary at the trailing edge hinge-line. The result of this situation is a loss of effectiveness for the trailing edge flap. The separation on the upper surface of the flap is clear in the skin friction plots of Figure 9 through Figure 12. Even more interesting is the fact that there is no indication that the shock may shift forward and allow the flow to separate forward of the hinge-line.

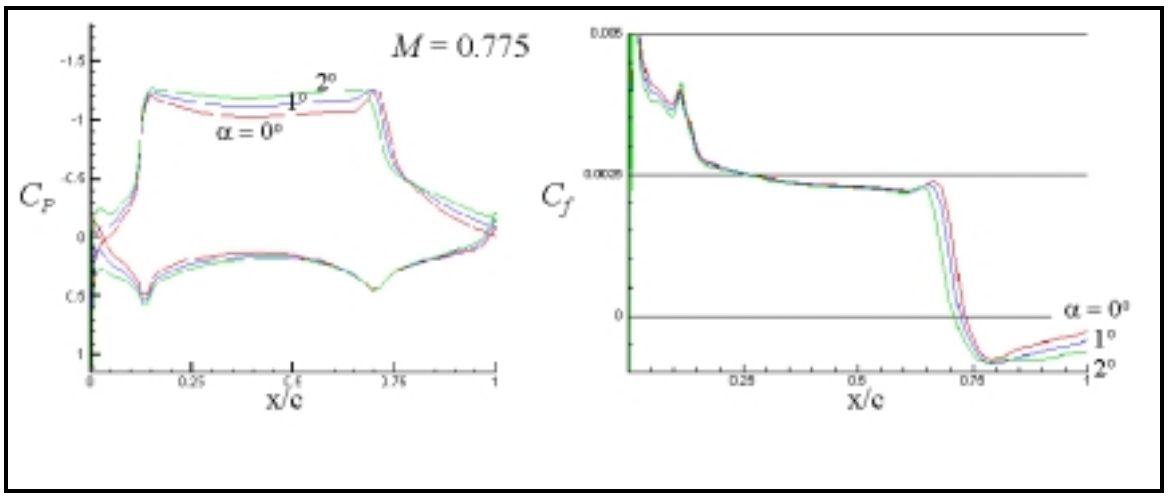

Figure 11. C_P and C_f vs α (M0.775)

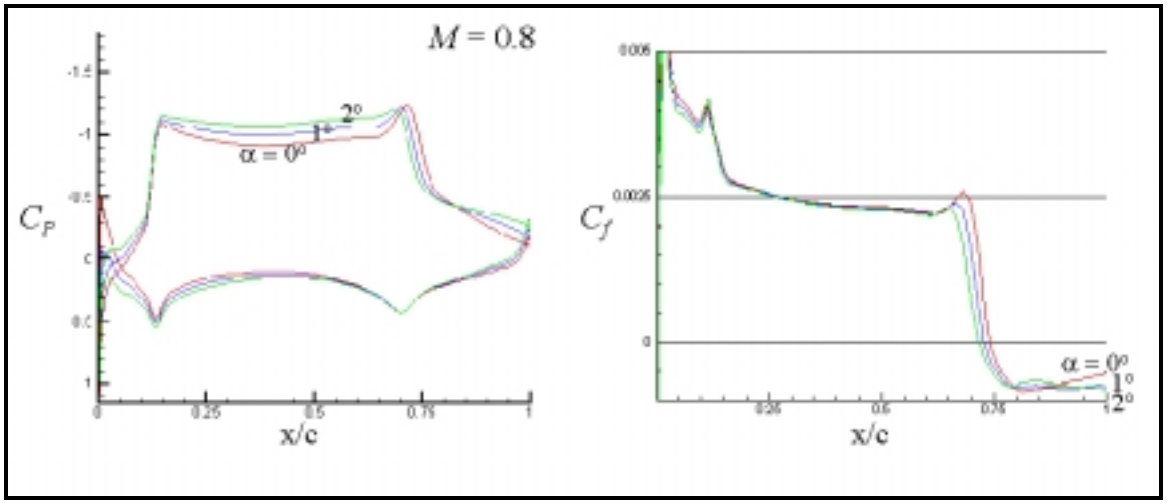

Figure 12. C_P and C_f vs α (M0.8)

The skin friction plots show fairly clearly where the flow is separated, and if the flow remains separated. However, it is helpful to see the effect the separation is having on the flow. The streamtrace plots seen in Figure 13 show how the flow has changed due to the separated region on the flap surface. Notice how the streamlines are pushed upward as the separation grows.

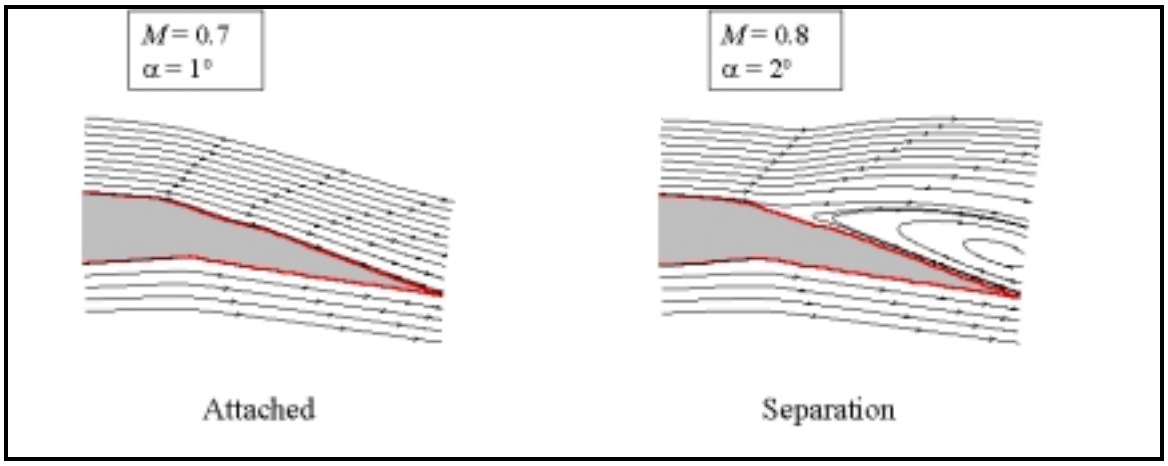

Figure 13. Streamlines over the trailing edge flap

The previous data summarizes the flow characteristics in response to the variation of angle of attack, for fixed Mach numbers. Even though the data has already been plotted in the previous plots, it is necessary to compile and compare the behavior of the flow with respect to changing Mach number. Holding angle of attack constant and varying the Mach number reveals similar results to that shown above.

Figure 14 shows the effect of Mach number at $\alpha=0^o$. Even for an angle of attack as low as 0^o, only the two lowest Mach numbers produce a shock that is located forward of the trailing edge hinge-line. The C_P distributions for $M0.7$ and $M0.725$ show the migration of the shock wave towards the trailing edge. Again, once the shock wave reaches the trailing edge hinge-line it becomes fixed and is altered little by increasing Mach number. The C_f plot on the right hand side reveals the development of separation on the flap for Mach numbers greater than 0.725. There appears to be no separation occurring in front of the trailing edge hinge-line.

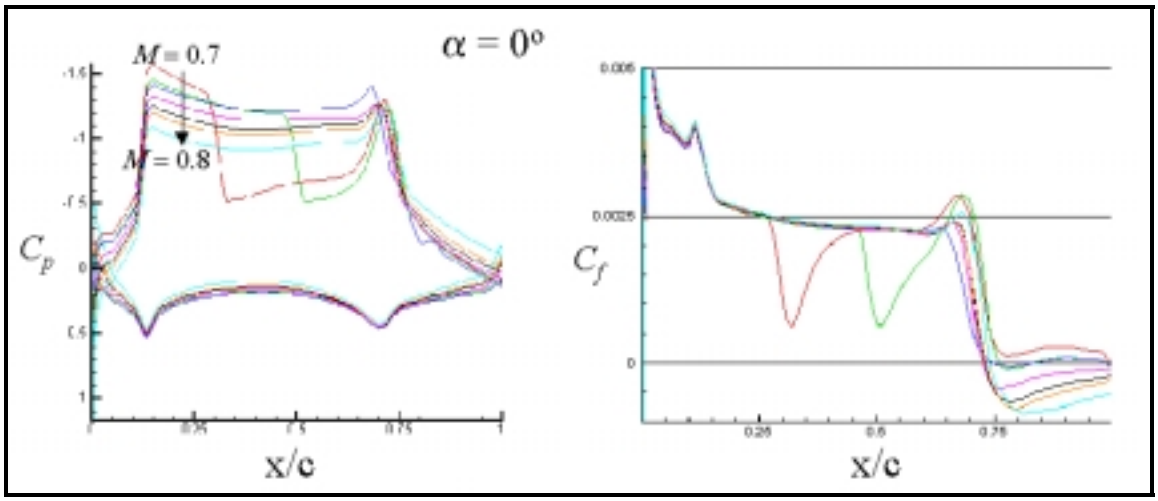

Figure 14: C_P and C_f vs M ($\alpha = 0^o$)

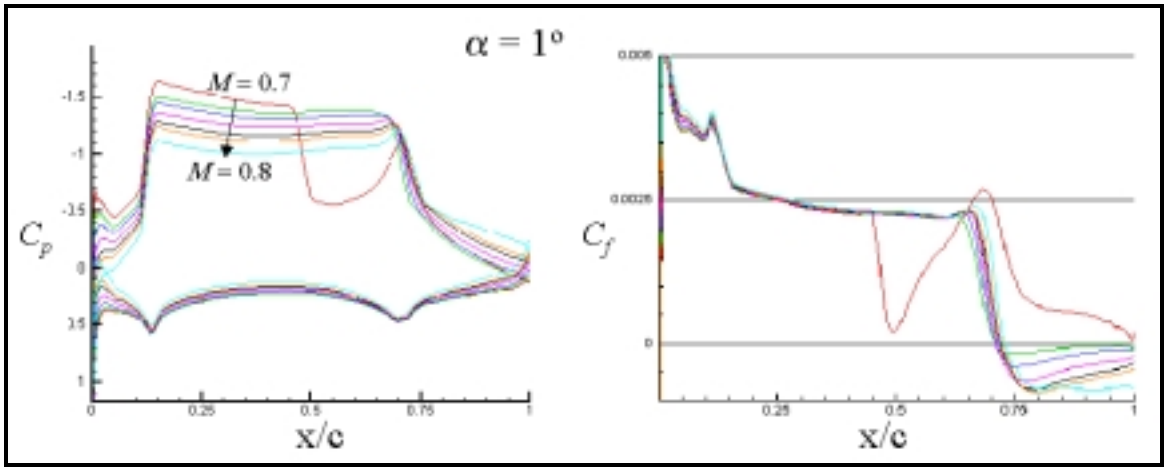

Figure 15. C_P and C_f vs M ($\alpha = 1^o$)

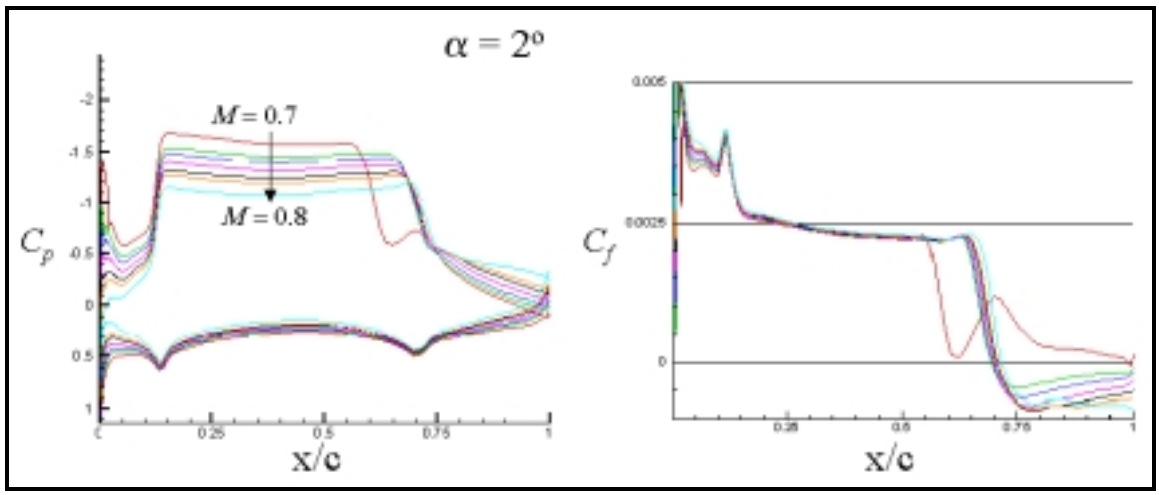

Figure 16. C_P and C_f vs M ($\alpha = 2^o$)

Figure 15 and Figure 16 confirm conclusions from Figure 14. The shock continues to shift rearward on the surface of the airfoil, and eventually all cases have a *Cp* profile similar to the ones seen in Figure 16. The large region of supersonic flow covers the entire section of the airfoil between the leading and trailing edge hinge-lines. As for separated flow, it appears that above an α of 0^o the only flow that remains attached for the entire airfoil is the *M*0.7 case. All higher Mach numbers show separated flow through the negative C_f values. It is important to notice that once again all separation is confined to the surface of the flap, or aft of the trailing edge hinge-line.

Chapter 5: Airfoil Comparison

Standing alone, the data from the NACA 65A005.7 airfoil does not provide a complete story on the relative sensitivity of the airfoil. To gain more conclusive information, it is necessary to do a comparative study of the airfoil. In order to limit the number of variables, the airfoil that was extracted for comparison purposes was also from a similar moderately swept wing. The comparative airfoil is a 3.5% thick NACA 65A series airfoil with a leading edge deflected at 6.34^{o} and a trailing edge deflected at 8.4^{o}. These device deflection angles were obtained from a control log written for this particular aircraft. Figure 17 shows the two 65A series airfoils.

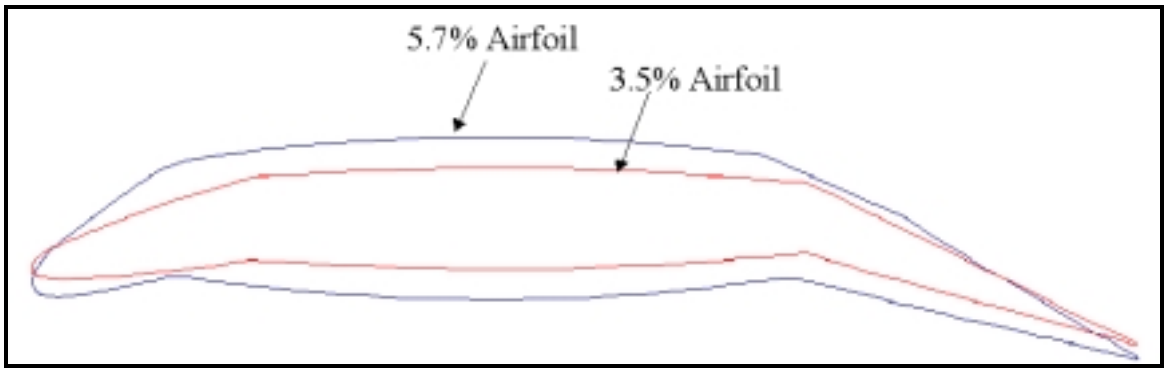

Figure 17: NACA 65A series airfoils

The airfoils shown in Figure 17 are not shown to scale, the thickness is exaggerated to better show the thickness and control surface differences. With this in mind it is important to note that the ‘corners’ formed at the control surface hinge-lines are not as profound as they appear in this figure. However, the effects of these geometric features on the airflow are significant, as seen in the previous chapter.

The geometry of the airfoils alone gives some indication that there will be a notable difference in the behavior of the flow pattern. This is verified by examining the C_P distributions for both airfoils at several angles of attack and Mach numbers.

Figure 18 introduces the flow characteristics of the 3.5% airfoil and its relation to that of the 5.7% airfoil. The first difference that one might notice is the behavior of the flow at the leading edge of the airfoil. The thinner airfoil obviously has a sharper leading edge than that of the 5.7% airfoil, in addition to a smaller deflection angle of the leading edge control surface. As a result, there is a more dramatic expansion and recompression near the leading edge. Similar to the 5.7% airfoil, the comparative airfoil has a notable pressure expansion at the leading edge hinge-line, followed by a recompression at some point downstream. As discussed in the previous chapter, the shock and thus the recompression is progressing towards the trailing edge of the airfoil as the angle of attack is increased.

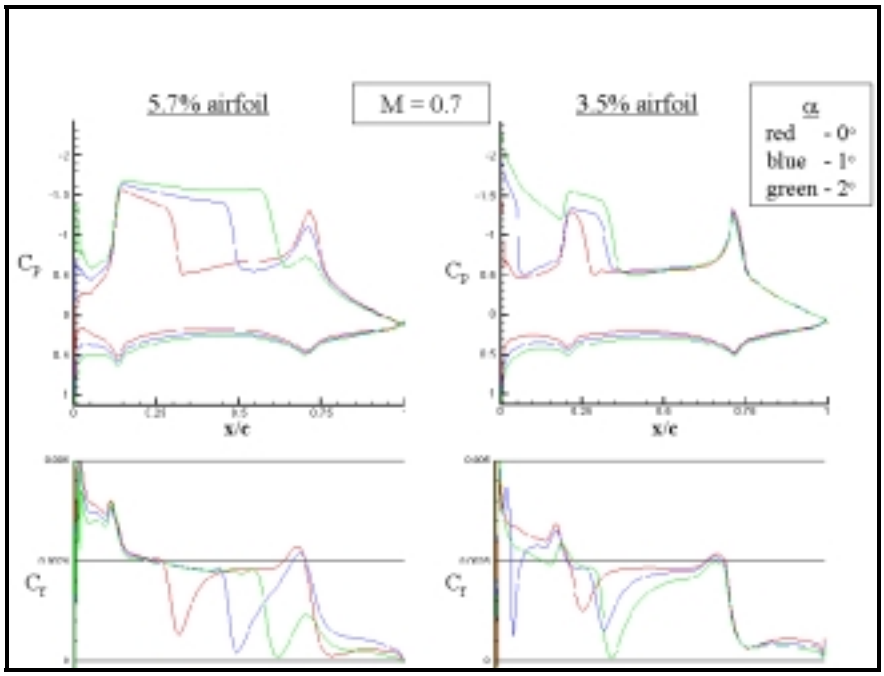

Figure 18. C_P and C_f vs. α comparison (M0.7)

As Mach number is increased, the effect on the thinner airfoil is similar to that of the 5.7% airfoil, as shown in Figure 19. The supersonic region in front of the shock wave is becoming noticeably larger as the shock is pushed aft. As a result, the airfoil is producing a larger C_l value. There is a sharp expansion and recompression located at the trailing edge hinge-line of the 3.5% airfoil. For α's of 0^o and 1^o there appears to be a slight separation bubble behind the trailing edge hinge-line. As the shock nears the hinge-line, the expansion/recompression here is reduced, and separation is nonexistent.

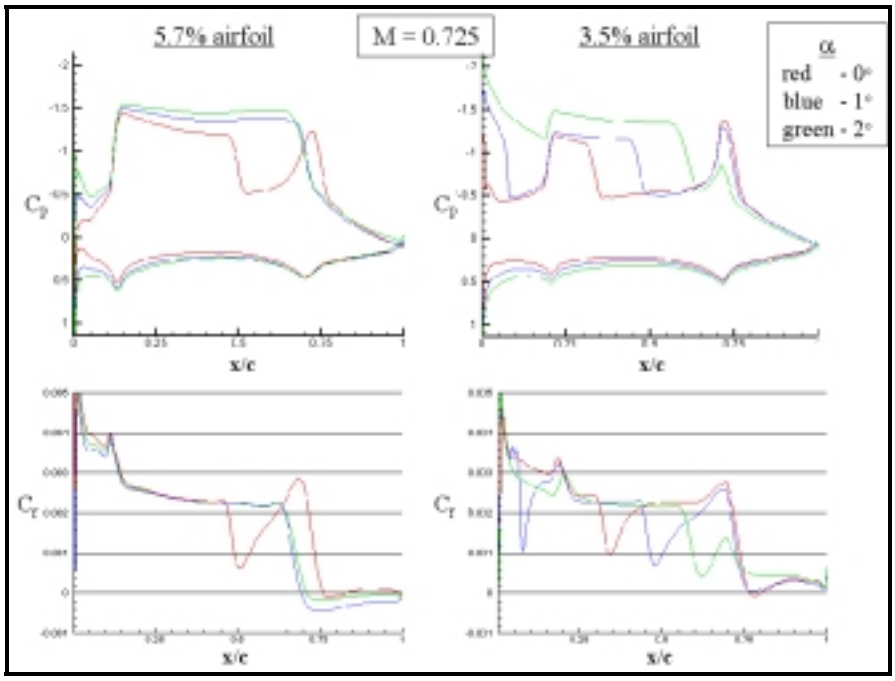

Figure 19. C_P and C_f vs α comparison (M0.725)

The plot displayed in Figure 20 shows what might be called the 'fully developed' C_P distribution for the 5.7% airfoil. The shock has become fixed at the trailing edged hinge-line for all cases of α that are higher than 0^o. In addition, the flow on the trailing edge flap has become separated. In comparison, the thinner airfoil for these conditions exhibits a C_P profile very similar to the 5.7% results seen in Figure 19, and it's progression is unmistakably the same. The C_f plot in Figure 20 for the 3.5% case is beginning to indicate separation in the flow over the trailing edge control surface.

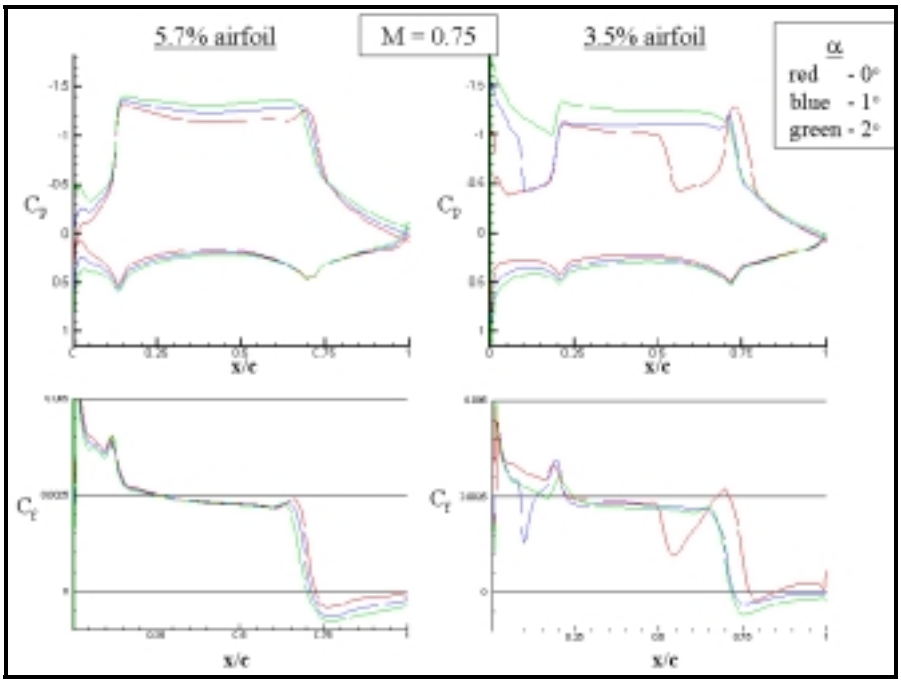

Figure 20. C_P and C_f vs. α comparison (M0.75)

The progression for the thinner airfoil is unmistakable, and the final result is nothing less than could be expected. In Figure 21 the C_P distribution for the 3.5% airfoil indicates that that the shock has migrated to the trailing edge hinge-line, and remains fixed for all three angles of attack. To confirm the stability of the shock at this position, Figure 22 shows the results for an even higher Mach number. In this figure the results for the 5.7% and 3.5% airfoil exhibit an unmistakable similarity in pressure distribution across the surface and flow separation on the trailing edge flap.

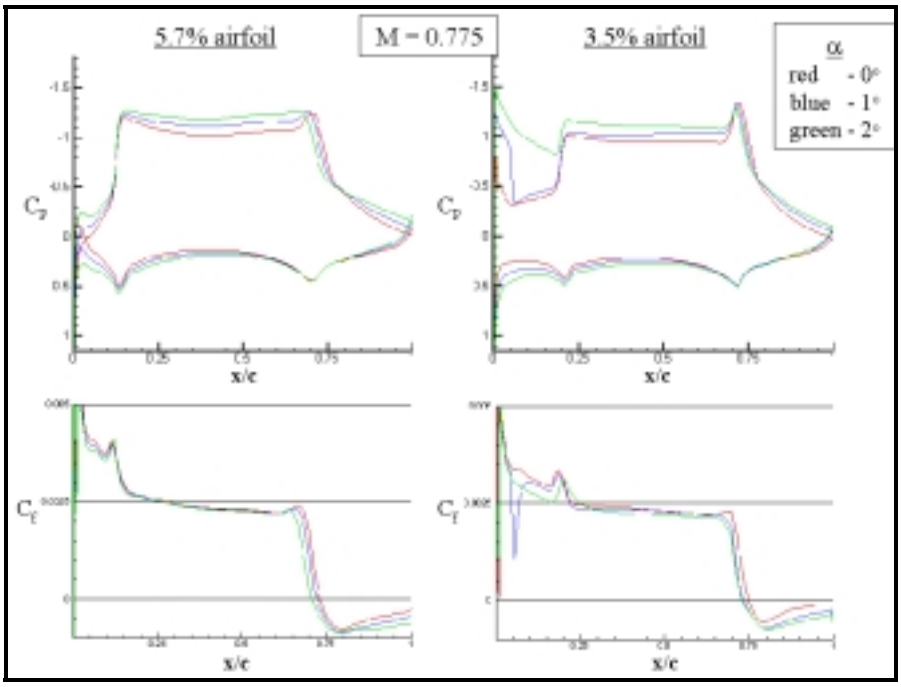

Figure 21. C_P and C_f vs. α comparison (M0.775)

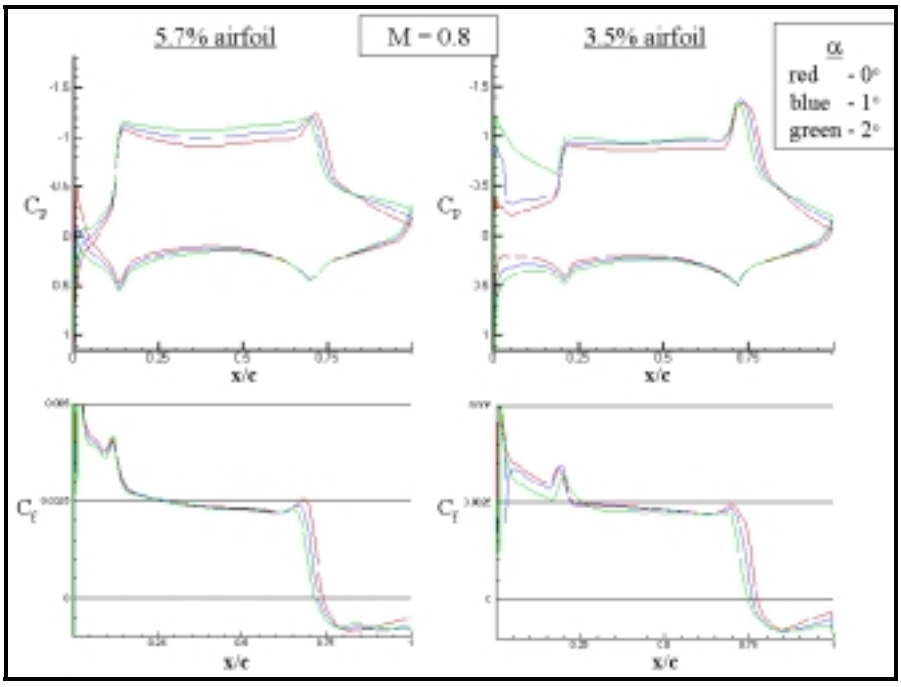

Figure 22. C_P and C_f vs. α comparison (M0.8)

It is difficult to draw any significant conclusions from this particular comparison, primarily because there is no sign of unconventional behavior or dramatic difference between the two airfoils. The main variation in the behavior of the flow over the two airfoils is in the rate of

development. The flow characteristics of the thinner airfoil at given conditions resemble characteristics of the 5.7% airfoil at a lower Mach number or angle of attack. The thicker, 5.7% airfoil reaches the “fully developed” state at a lower Mach number and angle of attack than the 3.5% airfoil. Particularly, the migration of the shock on the thicker airfoil is a step ahead of the thinner airfoil. This variation could be contributed to something as simple as the thickness difference in the airfoils. Regardless, this is not the level of variation that is of interest. Consistent variations are not of concern to this investigation, it is *abrupt* or *opposing* characteristics that are of interest.

Chapter 6: Significance of Control Surface Deflections on Shock Movement

The progression of the C_P distributions shown from the two-dimensional analysis have not resembled the data from the 3D CFD analysis. The C_P distribution for the NACA 65A airfoils described in chapter 4 have maintained an aft moving shock wave that becomes fixed on the trailing edge hinge-line. The result is a region of separation restricted to the trailing edge control surface. This is clearly not what has been exhibited by the three-dimensional analysis of the wing. A plot of the shock migration with respect to alpha in Figure 23 reveals the opposing results.

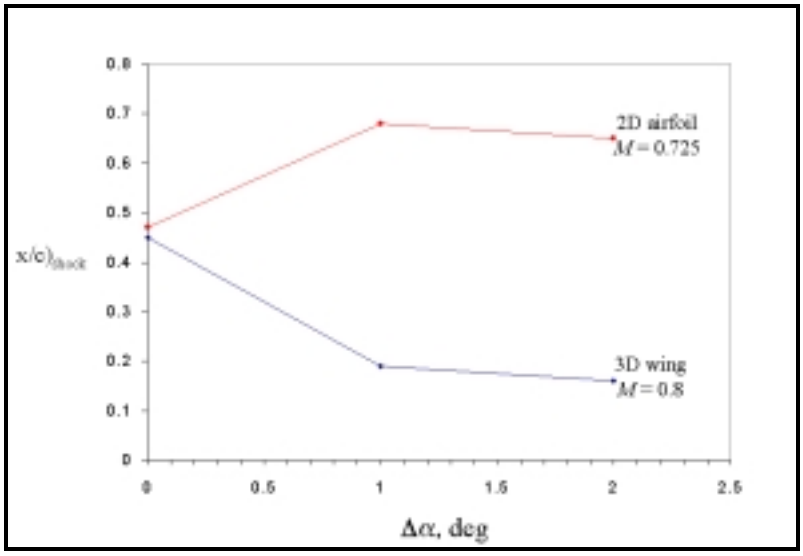

Figure 23. 2D vs. 3D shock movement

From Figure 23 it is clear that something significantly different is occurring between the two-dimensional and three-dimensional cases. One thing that can not be ignored is the fact that the shock continually becomes fixed at the trailing edge hinge-line for the two-dimensional cases. This occurrence sparks an interest in the effect of the trailing edge deflection. The leading edge and trailing edge control surfaces give the basic symmetric airfoil camber. In comparison an analysis was done on the NACA 65A005.7 airfoil without deflections.

Figure 24 shows the relation between the uncambered and cambered airfoils used in the analysis. Note the trailing edge hinge-line. The figure shown here is not to scale, the thickness is exaggerated to emphasize the deflections.

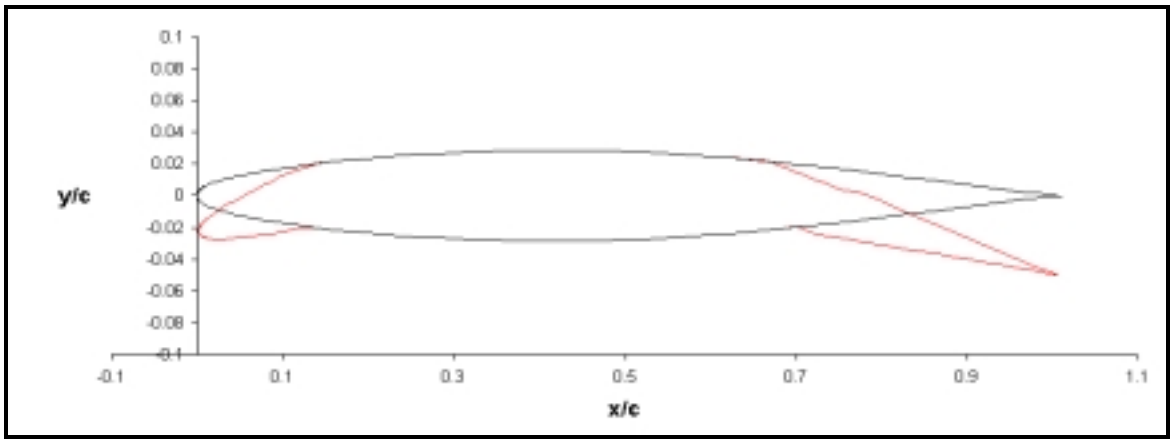

Figure 24. NACA 65A005.7 with and w/o deflections

Several cases were examined for the uncambered model of the airfoil. The results are plotted in Figure 25 and summarize the behavior without deflected surfaces. At low angles of attack, the shock begins to move steadily aft on the tail of the airfoil. The behavior is similar to that of the cambered case, at least until the angle of attack reaches 6^{o}. For alphas greater than 6^{o} there is a noticeable change in the shock migration. At this point the shock is actually moving forward on the airfoil. Obviously there is no hinge-line on this airfoil, and the shock does not become fixed at one location.

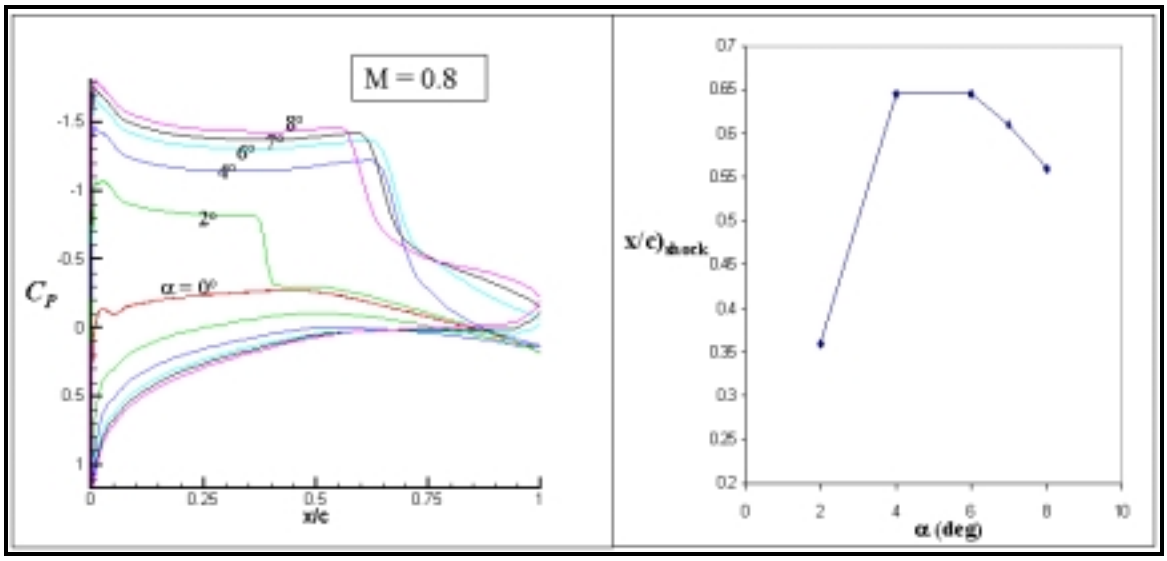

Figure 25. C_P & shock behavior for NACA 65A005.7 w/ no deflections (M0.8)

These results indicate a shock movement opposing that which has been exhibited by the original airfoil with flap deflections. In an attempt to understand this difference, the streamtraces were examined for select cases, as seen in Figure 26.

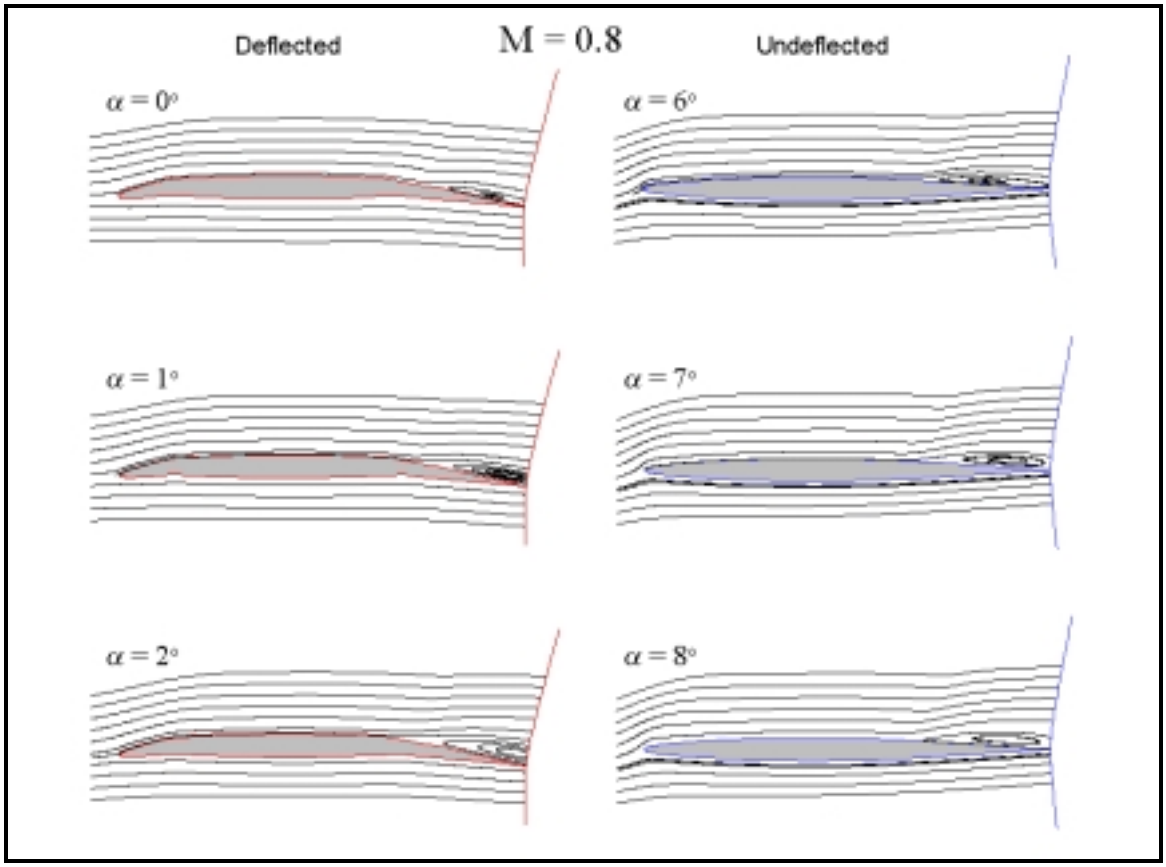

Figure 26. Streamtraces for cambered and uncambered airfoils

The first thing one may notice about the comparison in Figure 26 is the difference in the angles of attack used for the two airfoils. The reason for this is based on the location of the shock as seen in Figure 27. At this Mach number the shock on the cambered airfoil has become fixed at the trailing edge hinge-line for alphas as low as 0^o. Similarly the shock on the uncambered airfoil reaches its aftmost position around an alpha of 6^o. In other words, it was desired to compare the streamtraces of the cases where the shock has reached its aftmost position. For the cambered airfoil, this occurs around $\alpha=0^o$, 1^o and 2^o, for the uncambered airfoil it occurs around $\alpha=6^o$, 7^o and 8^o.

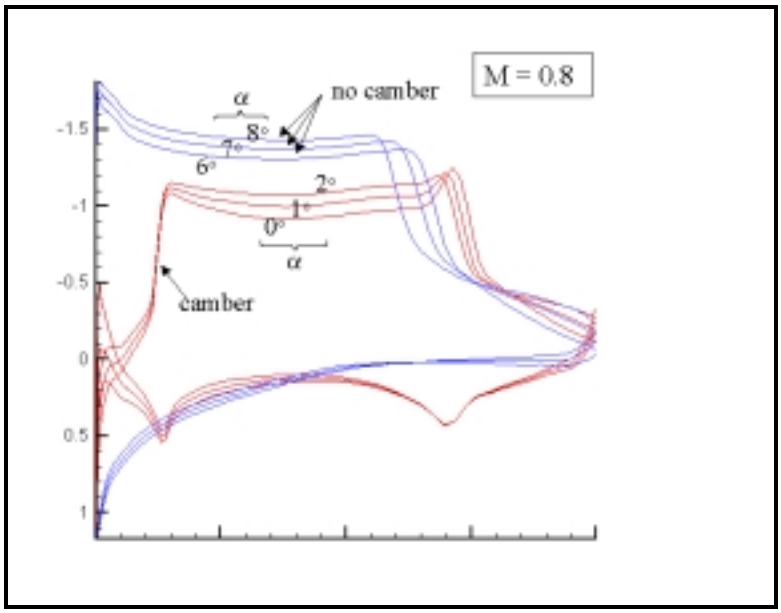

Figure 27. Cp comparison for camber & no camber

The reason for investigating the streamtraces displayed in Figure 26 is to gain an understanding of the *forward* migration in the shock on the uncambered airfoil. Obviously as the angle of attack is increased for these airfoils, the separation region grows. It is visible in Figure 26 that the thickness of the separation bubble is becoming larger, and the inviscid flow is forced upward. However, comparing the cambered and uncambered airfoil shows that the inviscid flow on the upper surface of the uncambered airfoil is effected more dramatically than that over the cambered airfoil.

As far as the inviscid flow is concerned, the increase in the size of the separation bubble is nothing more than a shape change, or an altered geometry. Since the separation bubble is increasing on both the cambered and uncambered airfoil, why is the shock moving forward only on the uncambered airfoil? The answer may lie in the relativity of the shape change. It may help

to examine the streamtraces with respect to a line drawn horizontal from the maximum aft location of the shock, as in Figure 28.

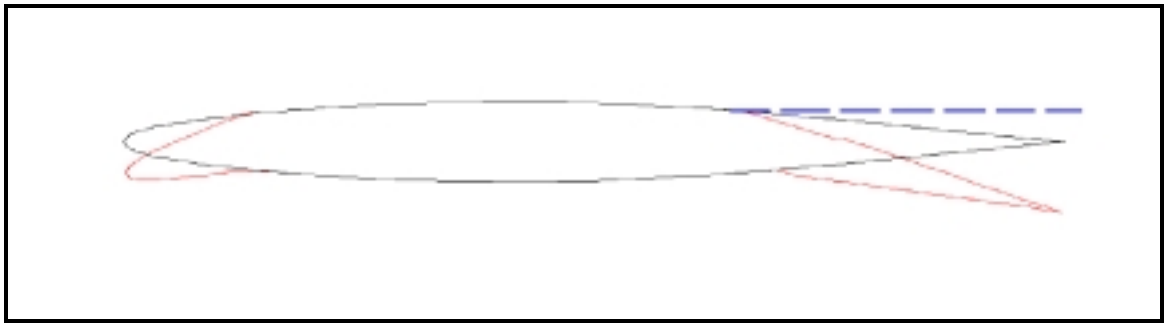

Figure 28. Cambered and uncambered airfoils

If this line were visualized in the plots of Figure 26, it would be clear that the separation region has a greater effect on the inviscid flow above the uncambered airfoil. With the flap deflected downward, there is an initial low pressure region encountered by the inviscid flow. As the separated region grows, the streamlines approach the horizontal line. As a result, the inciscid flow does not encounter the low pressure region caused by the deflected surface, and the effect on the shock location is minimal. As for the uncambered case, the increasing separation region rises above the horizontal line and causes the inviscid flow to push upwards, and the separation moves forward. The effect is visible in the streamtraces of Figure 26. The inviscid flow encounters the separation region as a 'hump' in the geometry. As a result, the shock is pushed forward.

The concept here is relatively simple, but the conclusion is profound. This behavior is nothing new, and the shock movement is as expected, but the implication is of interest. The fact that the shock doesn't move forward of the hinge-line in the two-dimensional analysis is an indication that the forward migration of the shock seen in the three-dimensional case is primarily a three-dimensional phenomenon. From the results shown in this chapter, it appears that the only way that the shock could jump forward of the trailing edge hinge-line would be for the flow to be forced to separate in front of the hinge-line. Of course, this is a two dimensional analysis. For a three-dimensional wing, spanwise flow can separate and alter the two-dimensional results.

Chapter 7: Conclusion

It's easy to disregard the results of a two-dimensional analysis on the basis that in a wing the flow is entirely three-dimensional. However, the purpose of this investigation was an attempt to isolate the source of the abrupt wing stall. The two-dimensional airfoil is a key component in the wing, and its characteristics remain prevalent even in the three-dimensional wing, especially considering the low sweep and two-dimensional type isobars. Therefore, if the airfoil used in the wing is prone to abrupt shock movements, the wing will likely retain the same characteristics.

The NACA 65A series airfoil of 5.7% thickness did not exhibit any tendency to abrupt shock movement. The aft movement of the shock was steady with increasing Mach number or increasing angle of attack. Supercritical expansion at the hingeline of the leading edge control surface is prevalent for all conditions. Following the expansion in each case is a sharp pressure recovery identifying the location of the shock. Eventually, as the shock shifts rearward, it becomes fixed on the trailing edge hingeline. An understanding of this behavior may be found in the work of Mason[3], but regardless of the explanation, this is where the shock remains as the flow separates over the flap.

In comparison with a similar airfoil, one extracted from a wing which does not exhibit wing stall characteristics, the results show similar patterns, but at different flow conditions. The shock behavior on the two airfoils is very similar, with the main difference most likely the result of thickness variation. In both cases, the shock eventually migrates to the trailing edge hingeline, where it becomes fixed for a reasonable range of Mach numbers and angles of attack. It can be concluded from this comparison, that the NACA 65A005.7 airfoil is not exceptionally sensitive to shock movement. There is no evidence of abrupt or opposing characteristics between the two comparative airfoils.

The fact remains that there is a definite disagreement between the motion of the two-dimensional shock and the three-dimensional shock (see Figure 23). An understanding of this difference was obtained from the comparison between the 5.7% airfoils with and without

deflected control surfaces. The deflection of the trailing edge flap allows the separation region to grow with a minimum effect on the upper surface inviscid flow. Typically the inviscid flow encounters a separation bubble as a shape change on the airfoil. As a result the shock in front of the separation region is pushed forward as the separation region grows. With the trailing edge deflected, the effect on the inviscid flow is reduced and the shock remains at the trailing edge hingeline. This does not explain why the shock behaves differently for the three-dimensional case, but it verifies that the forward movement of the shock is a three-dimensional phenomenon.

References

[1] Traven, R., Hagan, J., Niewoehner, R., "Solving Wing Drop on the F/A-18E/F Super Hornet," Society of Experimental Test Pilots' Symposium Proceedings, Lancaster, CA, 1998, pp. 67-84.

[2] Rathert, G. A., Jr., Rolls, S. L., Winograd, L., and Cooper, G. E., "Preliminary Flight Investigation of the Wing-Dropping Tendency and Lateral-Control Characteristics of a 35^{o} Swept-Wing Airplane at Transonic Mach Numbers," NACA RM A50H03, Sept. 1950.

[3] Mason, W.H., "Fundamental Issues in Subsonic/Transonic Expansion Corner Aerodynamics," AIAA Paper 93-0649, Jan. 1993.

[4] Greff, E., "Aerodynamic Design and Integration of a Variable Camber Wing for a New Generation Long/Medium Range Aircraft," International Council of the Aeronautical Sciences, Paper 88-2.2.3, Aug. 1988.

[5] Chung, Kung-Ming, "Transition of Subsonic and Transonic Expansion-Corner Flows," *Journal of Aircraft*, Vol. 37, No. 6, 2000, pp. 1079-1082.

[6] Ladson, C.L., and Brooks, C.W., Jr., "Development of a Computer Program to Obtain Ordinates for NACA 6- and 6A-Series Airfoils," NASA TM X-3069, Sept. 1974.

[7] Swanson, R. C, personal contact, June 2000.

[8] Swanson, R. C., Turkel, Eli, "Multistage Schemes with Multigrid for Euler and Navier-Stokes Equations: Components and Analysis," NASA-TP-3631, Aug. 1997.

[9] Baldwin, B. S., and Lomax, H., "Thin Layer Approximation and Algebraic Model for Separated Turblulent Flows," AIAA Paper 78-257, Jan. 1978.

[10] Johnson, D. A., and King, L. S., "A Mathematically Simple Turbulence Closure Model for Attached and Separated Turbulent Boundary Layers," *AIAA Journal*, Vol. 23, 1985, pp. 1684-1692.

[11] Johnson, D. A., and Coakley, T. J., " Improvements to a Nonequilibrium Algebraic Turbulence Model," *AIAA Journal*, Vol. 28, 1990, pp. 2000-2003.

[12] Londenberg, W. K., "Turbulence Model Evaluation for the Prediction of Flows Over a Supercritical Airfoil with Deflected Aileron at High Reynolds Number," AIAA Paper 93-0191, Jan. 1993.

[13] Londenberg, W. K., "Turbulence Model Evaluation for Use with Supercritical Airfoils," *AIAA Journal*, Vol. 31, 1993, pp. 977-979.

[14] Holst, T. L., "Viscous Transonic Airfoil Workshop Compendium of Results," *Journal of Aircraft*, Vol. 25, No. 12, Dec. 1988, pp. 1073-1087.

Vita

Michael M. Henry was born in the heart of the Shenandoah Valley, in the a historic city of Staunton, Virginia, on December 17, 1976. He graduated from Grace Christian School in 1995 and attended Virginia Polytechnic Institute and State University for undergraduate studies. After four years of intense hunting, fishing, camping and studying he received his dual B.S. degree in aerospace and ocean engineering from Virginia Tech. In the fall of 1999 Mike began graduate research under Dr. W. H. Mason on the aerodynamics of the “wing drop” phenomenon. Two years later he completed his research, compiled in this report, and obtained his M.S. degree in aerospace engineering with a focus on aerodynamics.